A New Strategy for Fabricating Low Haze p-Type CuI Film

Ruisong You
Shandong University
Shulin Luo
Shandong University
Weixin Liu
Shandong University
Hui Sun (huisun@sdu.edu.cn)
Shandong University

Research Article

Keywords: Copper (I) iodide (CuI), low haze, p-type transparent conductive films, iodination

Posted Date: July 23rd, 2021

DOI: https://doi.org/10.21203/rs.3.rs-736842/v1

Abstract

As an intrinsic p-type transparent conductor with a wide band gap of 3.1 eV, γ-CuI full of potential has gradually attracted the attention of researchers. However, γ-CuI films deposited by various techniques generally present high haze with a frosted-glass-like appearance, significantly hampering the device's performance. Herein, a new strategy is proposed, where truly p-type CuI thin films with low haze were successfully synthesized at room temperature. The specular transmittance of CuI film above 85% in the visible region (400-800 nm) can be achieved. The haze of the as-prepared γ-CuI films can be as low as 0.7%. Meanwhile, the as-prepared CuI film possesses a FOM as high as 230 MΩ -1 . This ideal stable p-type optoelectronic performance was a significant achievement among various typical p-type transparent conductive films.

1. Introduction

Transparent conductive oxides (TCOs) can be widely used in passive and active electronic applications, such as flat-panel displays, photovoltaic devices, light-emitting diodes, smart windows, photo-detectors, *etc.* [1-4]. However, p-type TCOs as an essential component employed in the active devices, their performance is far behind n-type TCOs, seriously limiting the application of these active devices [2]. The discovery of the first p-type transparent semiconductor with application potential is $CuAlO_2$ [5], after which increasing attention was paid to Cu^I-based oxides, especially the oxides with delafossite structure. $CuMO_2$ with delafossite structure presents attractive p-type optoelectronic properties among various oxides [6-9]. Unfortunately, the figure of merit (FOM) of those kinds of materials is below 10 $M\Omega^{-1}$ [6-12]. Most recently, correlated metals $CaVO_3$ and $SrVO_3$ even their p-type doping materials such as $La_{2/3}Sr_{1/3}VO_3$ with high p-type conductivity about 742.3-872.3 $S{\cdot}cm^{-1}$ have been reported. Regrettably, their transmittance further deteriorates [13-15]. As a result, improving the conductivity of p-type TCOs meanwhile maintaining their high transmittance is indeed a great challenge at this moment.

γ-phase cooper iodide (γ-CuI), an inexpensive and non-toxic p-type semiconductor has attracted people's attention. It is an intrinsic p-type semiconductor with low hole effective mass (0.30 m_0) and high bulk hole mobility (>40 $cm^2{\cdot}V^{-1}{\cdot}s^{-1}$) [16,17]. Its wide direct band gap (E_g = 3.1 eV) is beneficial for the fabrication of transparent semiconductor; while its high exciton binding energy of E^b_x = 58 meV is also beneficial as it used in the optoelectronic devices [18,19]. In addition, n-type CuI can also be realized by doped with Zn [20], resulting in that the p-CuI/n-CuI homo-junction can be realized, further greatly broaden the application of CuI in various optoelectronic devices. γ-CuI films have been synthesized through various physical and chemical methods, such as sputtering [21], pulsed laser deposition (PLD) [22], solution method [23], thermal evaporation [24], and iodination method [25]. However, the γ-CuI films deposited by different techniques generally possess high haze with gross grains and present a frosted-glass-like appearance [16,26-28]. This feature increases the light scattering and seriously reduces the film's transmittance. At present, many efforts have been paid to reduce the haze of CuI filmand enhance the

film's transmittance. One of the most attractive means is preparation CuI films through iodination method, i.e., using different precursors such as Cu [25], Cu_3N [25], CuS [29] to react with iodide. In addition, Vidur Raj *et al.* also incorporated a second-phase such as TiO_2 into CuI films to inhibit the growth of CuI grain and lower the film's haze [30]. However, the results are unsatisfactory: the transmittance of CuI films with a thickness below 100 nm prepared by the above methods is still lower than 70%.

Consequently, novel strategy to fabricate γ-CuI film with high visible transmittance and low haze is necessary. In the current work, CuI films were prepared by the iodination of Cu_3N precursor. The film's haze as well as the surface morphology can be controlled by adjusting the contact area between iodine and the Cu_3N precursor. The transmittance of the as-prepared γ-CuI films can reach 86%. The haze of the as-prepared γ-CuI films can be below 0.7%. Benefit to the high transmittance, the figure of merit (FOM) of the optimal CuI film above 230 $M\Omega^{-1}$ can be realized.

2. Experimental Section

2.1. Fabrication of the Precursor Cu_3N Thin-Film

2.5 cm × 2.5 cm glass substrates were cleaned with acetone in an ultrasonic bath then dried with N_2. Next, the Cu_3N thin films were deposited on glass substrates from the copper target (purity of 99.99%) by reactive radio frequency (RF) magnetron sputtering. The sputtering power maintains at 80 W. The background vacuum of the sputtering chamber was 5×10^{-5} Pa. Before the deposition, the copper target was pre-sputtered with pure Ar for 10 min to remove the oxide layers from the target surface. The deposition pressure is 0.8 Pa with argon flow of 40 sccm and nitrogen flow of 20 sccm. The thickness of the Cu_3N precursor is about 75 nm.

2.2. γ-CuI Thin Film Fabrication

γ-CuI thin films were fabricated via the chemical reaction between Cu_3N precursor films and liquid, vapor or solid-phase iodine:

$$2Cu_3N + 3I_2 \rightarrow 6CuI + N_2 \qquad (1)$$

The liquid, vapor, and solid iodination procedures are schematically illustrated in Fig. 1. Fig. 1a shows the liquid iodination process. First, 0.1 g iodine particles and 0.2 g KI powder were dissolved in 100 ml water as iodine aqueous solution. 5 ml iodine aqueous solution was transferred into a petri dish. Cu_3N precursor was immersed in an iodine aqueous solution at room temperature. The iodination reaction maintains 5 min. Fig. 1b shows the vapor iodination process. Iodine particles were distributed evenly at the bottom of the petri dish. Cu_3N precursor films were buckled on the petri dish and faced towards iodine vapor. Then, the petri dish was kept at room temperature for 5 min. Fig. 1c shows the solid iodination

process. The Cu_3N precursor films were placed face up in a petri dish. The Cu_3N film was fully covered with iodine particles for 5 min. The diameter of CuI particles is about 2.5mm.

For the solid iodination method, the different arrangements of contact area and non-contact area were realized by controlling the amount of iodine particles (density of iodine particles) on the surface of Cu_3N precursor. The low haze sample was prepared by the Cu_3N precursor fully covered with iodine particles, and the sample with medium haze was prepared by placing 1/2 iodine particles of the low haze sample on the Cu_3N precursor surface of the sample. High haze samples were prepared by evenly placing 1/2 of iodine particles on the surface of Cu_3N precursor.

2.3. Characterization.

The transmittance and reflectance of CuI thin films were measured using a PerkinElmer UV-visible-IR spectrophotometer in the wavelength range of 200–2000 nm. The phase structures of the films were analyzed through an X-ray diffractometer (XRD, Rigaku Ultima IV, Japan) with Cu anode (λ = 0.154 nm). The surface morphology and cross-sectional morphology of the films were observed with a field emission scanning electron microscope (FE-SEM; Nova Nano SEM 450, USA). The films' surface roughness was detected by atomic force microscope (AFM; SPI3800N, SII). The resistivity (ρ), carrier concentration (n_h), and carrier mobility (μ) of the films were determined by Hall effect measurements in the van der Pauw configuration (Keithley-4200 SCS, USA) at room temperature. The electrical resistivity of the films under bending was measured by the four-point probe method (RTS-8, China). Haze and CIELAB color values were measured by a spectral haze meter (HAM-300, China).

3. Results And Discussion

Top-view SEM images of γ-CuI thin films fabricated by different iodination methods are presented in Fig. 3a-c. AFM images of γ-CuI thin films fabricated by different iodination methods are presented in Fig. 4a-c. The Vis-IR spectra of CuI films prepared through liquid, vapor, and solid iodination methods are shown in Fig. 5a. The photographs for liquid, vapor and solid iodination methods are shown in Fig. 5b. The CuI thin films fabricated by the liquid and vapor iodination methods have both low reflectivity and low transmittance. It can be explained by SEM and AFM images of CuI films. As shown in Fig. 3a and Fig. 4a, the CuI film fabricated by the liquid iodination has a lot of huge and spares grains and roughness surface. When a beam of light irradiates a thin film with many cracks, the light will be scattered and propagate in other directions [25]. Therefore, the transmitted light and the reflected light intensity detected by the detectors are both weak. For this reason, the reflectance and transmittance are both lower as shown in Fig. 5a.

Those factors increase the reflecting and scattering of incoming light and give a milky appearance as shown in Fig. 5b. The CuI film fabricated via the vapor iodination method is slightly better than the liquid method. But the film fabricated by vapor iodination has a rough surface with obvious empty spaces as shown in Fig. 3b,e, and Fig. 4b. Therefore, the film has a frosted-glass-like appearance as shown in Fig.

5b. In contrast, those grains of the CuI film fabricated by the solid iodination are significantly smaller and denser as shown in Fig. 3c,f. Those small and dense grains will lead to a smooth surface as shown in Fig. 4c. The light transmittance of the γ-CuI films fabricated by solid iodination is higher than others due to minimizing incoming light reflecting and scattering by the smooth surface of films. Therefore, the CuI film fabricated by the solid iodination method has both the highest transmittance and strong Fabry–Pérot interference as shown in Fig. 5a.

In addition, pronounced excitonic absorption is visible at $E_{Z1/Z2}$ = (3.05 ± 0.01) eV. Transitions due to spin-orbit coupling apparent at E_{Z3} = (3.68 ± 0.01) eV. The E_g of γ-CuI can be calculated by adding $E_{Z1/Z2}$ to the excitonic binding energy [19,22]. The E_g obtained by those three methods is ~3.10 eV, which is consistent with theoretical calculations and other experimental reported [16,19,24]. The absorption coefficient was calculated by the Beer-Lambert relation

$$\alpha = \frac{1}{t} ln(\frac{1}{T}) \qquad (2)$$

where t is the thickness and T is the transmittance. The spectra of absorption are consistent with the spectra in another report. The applicable condition of the Beer-Lambert relation is a non-scattering system. The films we fabricated via liquid and vapor iodination methods have obvious scattering. Therefore, the α has a significant shift as shown in Fig. 5c.

In this study, the solid-state reaction is used to explain the obvious difference of CuI films prepared by iodization. Generally, the solid-state reaction is divided into two processes: reaction between interface and diffusion of reactive species in the precursor. Jander's equation is one of the most popular to examine solid-state reaction kinetics under isothermal conditions [33,34]. Its expression is

$$\left(1-\sqrt[3]{1-\alpha}\right)^2 = \frac{2Dc_0}{r^2} \cdot t = k' \cdot t \qquad (3)$$

where α is the conversion rate of reactants, D represents the diffusion coefficient, c_0 represents the reactant concentration at the interface between the layer of reaction products and the reactant, t represents the time and r is the spherical reactant particles' radius.

A diagram of the growth of the CuI grains basing on Jander's equation and intuitive results was proposed as illustrated in Fig. 6. Compared with the solid iodization method, the liquid and vapor iodination methods have many iodine molecules in contact with the Cu_3N precursors, which makes the interface reaction area larger. Meanwhile, iodine aqueous solution and iodine vapor have lower concentrations at the reaction interface than solid iodine particles, which makes all reactions slower. Each contact point reacts with the precursor at the same time, so that there is already a layer of CuI on Cu_3N grains as shown in Fig. 6a. When the outer "shell" of the grain was formed, the process of further diffusion-reaction is the iodination reaction inside the precursor. Therefore, the CuI film has coarser grains. The coarse grains can cause empty spaces as shown in Figure 3a,b. On the contrary, the CuI film fabricated by solid iodination

has small grains instead of shell layers due to the few contact area between the iodine solid particles and the Cu_3N film as shown in Fig. 5b. The iodination process of non-contact points grows freely with the diffusion of iodine atoms without the influence of the CuI “shell” layer, so the grains are smaller. Fortunately, the arbitrarily distributed small grains make the film more compact.

3.2. A New Strategy

Based on the above analysis, we infer the key factor to improve the transmittance of CuI films is to reduce the grain size to form a denser film structure with a smooth surface. A denser film structure with a smooth surface can reduce the light scattering of CuI films. The effect of solid iodization is the best among the three iodization methods, and the details of solid iodization are studied.

When iodine particles contact with Cu_3N precursor, they can be divided into contact areas and non-contact areas. Therefore, what are the similarities and differences between the two regions? The schematic diagram of Fig. 7a,b shows the preparation process of two cases. The contact area is prepared by completely covering the iodine powder. The iodine particles are placed on the edge of the precursor for iodization, and the middle area is the non-contact iodization area. The γ-CuI films fabricated by iodine particles contact iodination are smooth as shown in Fig. 7b,e. The root-mean-square (RMS) roughness of the 10 × 10 μm^2 scanned area was 9.8 nm. In contrast, the non-contact iodization areas of γ-CuI films have different surface morphology as shown in Fig. 7c. The root-mean-square (RMS) roughness of the 10 × 10 μm^2 scanned area was 27.1 nm. This can also be explained by the above analysis of solid-state reaction. As shown in Fig. 7d, the non-contact iodization area γ-CuI films have a frosted-glass-like appearance and a low transmittance (73%) due to small uneven grains on the substrate in the no-contact area, which is consistent with a previous report [25]. But the CuI grains generated in the contact area are very flat. Its average transmittance is as high as 85%. In other words, the reaction between the iodine solid particles and the Cu_3N precursor in the contact interface (contact iodination area) between solid-state iodine and Cu_3N precursor (noted as step1) is smoother than the reaction due to the diffusion (non-contact iodination area) of reactive species in the Cu_3N precursor (noted as step2). Therefore, the transmittance of step1 is higher than step2.

Improving film smoothness and grain density can reduce light scattering, and then increasing the transmittance of films and eliminating the frosted-glass-like appearance of the film. It has been reported that a high smooth surface will make the reflectivity too high and reduce the transmittance [25,35] so that the transmittance of CuI film obtained by solid iodization is only about 70% [25]. In this study, it is found that reflection has no obvious effect on CuI films prepared by solid iodination. This study proposed films with different roughness area distributions and selected three representative films for analysis.

Fig. 8a shows the schematic three arrangements and their scattering, green represents contact areas, gray represents the non-contact area. According to the haze and interference of prepared film, the distribution of the two areas of a sample is visible. Fig. 8b shows the transmittance and reflectivity of three arrangements. Fig. 8c shows the visible transmittance and haze of those films. Fig. 8d shows the

Lab color of those films. The negative value of the ‘a’ axis tends to green, and the positive value tends to red. The negative value of the ‘b’ axis tends to be blue, and the positive value tends to be yellow. When the distribution of smooth area is denser, the surface of CuI film is so smooth. The film has obvious Fabry Perot interference due to smooth surface as shown in Fig. 8b. The CIELab color values of a and b are less than 10 as shown in Fig. 8d. It indicates that the interference color does not affect its application as the transparent conductive film. In the visible region, CuI film has high transmittance and low haze due to the light scattering of the film is low. Although the reflectivity is slightly higher than other CuI films, the transmittance is still as high as 85%. When the uneven area is density, the CuI film has a high haze and low transmittance due to the rough surface of the CuI film. The haze is linearly correlated with the transmittance as shown in Fig. 8c. Therefore, the film with a smooth surface can be prepared by controlling the density of the contact area.

Different devices require different haze on the electrode. For example, the touch-panel displays require low haze transparent electrodes [36-38], but solar cells need transparent electrodes with high haze to improve light utilization [39-41]. Therefore, this strategy also can modify the haze of CuI film from 0.7% to 21% to meet the needs of different electronic devices. That will greatly expand the application of CuI as transparent conductive films.

3.3. Photoelectric performance of p-type TCs

Quantitatively, the overall photoelectric performance of the TC can be quantified by the Haacke figure of merit (FOM) [42], $\Phi_{TC} = T^{10}/R_s$ where T is the average transmittance in the visible region and R_s is the sheet resistance. A larger value of FOM indicates the better photoelectric performance of the TC. As shown in Table 1, the FOM of most novel p-type TCs is lower than 20 $M\Omega^{-1}$. In contrast, the as-deposited γ-CuI film shows a FOM about 11× higher, up to 233 $M\Omega^{-1}$, while providing a high T_{vis} above 86%. These results demonstrate the superior TC photoelectric performance of our γ-CuI films with respect to all measures.

Table 1. Transmittance, resistivity, and the FOM of CuI films and other p-type TCs

Materials	d (nm)	σ (S/cm)	Rs (kΩ/sq)	T_{vis} (%)	FOM ($M\Omega^{-1}$)	Referece
$Ca_3Co_4O_9$	100	18	5.5	31.3	0.0015	[43]
GaN: Mg	100	5.3	19	70	1.487	[44]
SnO	200	0.77	650	85	3.03	[45]
$Mg_xCr_{2-x}O_3$	150	0.333	200	65	0.067	[46]
$La_{2/3}Sr_{1/3}VO_3$	24	816.3	0.51	61.1	14.21	[14]
$CuAlO_2$	230	0.34	130	70	0.217	[12]
$CuGaO_2$	100	0.02	5000	80	0.022	[6]
$CuCrO_2$	180	0.19	292.4	58.3	0.015	[8]
$CuScO_{2+x}$	110	15	6.06	40	0.0173	[10]
$CuCrO_2$: Mg	50	1.55	129	49.81	0.123	[11]
CuI	230	45	0.95	86	233	This work

Figure 9 shows the transmittance, conductivity, and FOM values of CuI films prepared by the new strategy and other methods. The films prepared by the new strategy have better performance than other CuI films. Compared with other preparation methods, this new strategy is simple and controllable. Moreover, the haze can be adjusted from 0.7% to 22%. This expands the application range of CuI as the transparent conductive film.

4. Conclusion

In summary, we fabricated γ-CuI films via solid, vapor, and liquid iodination of Cu_3N precursors. The SEM and AFM images show the γ-CuI films fabricated by the solid iodination method have smaller and denser grains, fewer empty spaces, and lower surface roughness. Those factors lead to high transmittance, great electrical properties as well as better flexibility. Furthermore, we studied the contact and non-contact regions between the Cu_3N film and iodine particles in solid iodination. The SEM and AFM images show that the solid iodination method has two different steps with different surface morphology. They have obvious differences in light scattering. The first step is the reaction between the interface of Iodine granules and Cu_3N film. The second step is the diffusion of reactive species in the Cu_3N layer. Based on this phenomenon, a new strategy was proposed to fabricate high transmittance and low haze CuI films. The FOM of the CuI film prepared by this new strategy is >230 $M\Omega^{-1}$. Compared with other p-type transparent conductive materials and CuI films prepared by other methods, the photoelectric performance

of CuI film prepared by this strategy is excellent. Besides, this strategy can also make the haze of the CuI film controllable. This study can promote the application of CuI film in optoelectronic devices.

Declarations

Acknowledgments

We gratefully acknowledge the National Natural Science Foundation of China (No. 62004117), Young Scholars Program of Shandong University, Weihai for their financial support. We also thank the Physical-Chemical Materials Analytical & Testing Center of Shandong University at Weihai for their assistance with characterization.

References

1. J. Zhao, Z. Chi, Z. Yang, X. Chen, M. Arnold, Y. Zhang, J. Xu, Z. Chi and M. P. Aldred, Recent developments of truly stretchable thin film electronic and optoelectronic devices, Nanoscale 10 (2018) 5764-5792.
2. Z. Wang, P.K. Nayak, J.A. Caraveo-Frescas, H.N. Alshareef, Recent Developments in p-Type Oxide Semiconductor Materials and Devices. Adv. Mater 28 (2016) 3831-3892.
3. H. Hosono, Recent progress in transparent oxide semiconductors: Materials and device application. Thin Solid Films 515 (2007) 6000-6014.
4. E. Fortunato, P. Barquinha, R. Martins, Oxide semiconductor thin-film transistors: A review of recent advances. Adv. Mater 24 (2012) 2945-2986.
5. H. Kawazoe, M. Yasukawa, H. Hyodo, M.i Kurita, H. Yanagi & H. Hosono, p-type electrical conduction in transparent thin films of $CuAlO_2$. Nature 389 (1997) 939-942.
6. K. Ueda, T. Hase, H. Yanagi, H. Kawazoe, H. Hosono, H. Ohta, M. Orita, M. Hirano, Epitaxial growth of transparent p-type conducting $CuGaO_2$ thin films on sapphire (001) substrates by pulsed laser deposition. J. Appl. Phys. 89 (2001) 1790-1793.
7. H. Yanagi, T. Hase, S. Ibuki, K. Ueda, H. Hosono, Bipolarity in electrical conduction of transparent oxide semiconductor $CuInO_2$ with delafossite structure. Appl. Phys. Lett. 78 (2001) 1583-1585.
8. C. Sun, D. Tsai, Z. Chang, E. Chen, F. Shieu, Structural, optical, and electrical properties of conducting p-type transparent Cu–Cr–O thin films. Ceramics International 42 (2016) 13697–13703.
9. MK. Jayaraj, AD. Draeseke, J. Tate, AW. Sleight, p-Type transparent thin films of $CuY_{1-x}Ca_xO_2$. Thin Solid Films 397 (2001) 244-248.
10. N. Duan, AW Sleight, MK Jayaraj, J. Tate, Transparent p-type conducting $CuScO_{2+x}$ films. Appl. Phys. Lett. 77 (2000) 1325-1326.
11. S.S. Lin, Q. Shi, M.J. Dai, K.L. Wang, S.C. Chen, T.Y. Kuo, D.G. Liu, S.M. Song. H. Sun, The Optoelectronic Properties of p-Type Cr-Deficient Cu $[Cr_{0.95-x}Mg_{0.05}]$ O_2 Films Deposited by Reactive Magnetron Sputtering, Materials 13 (2020) 2376.

12. H. Yanagi, S. Inoue, K. Ueda, H. Kawazoe, H. Hosono, and N. Hamada, Electronic structure and optoelectronic properties of transparent p-type conducting $CuAlO_2$, J. Appl. Phys. 88 (2000) 4159-4163.
13. L. Zhang, Y. Zhou, L. Guo, W. Zhao, A. Barnes, H. Zhang, C. Eaton, Y. Zheng, M. Brahlek, Hamna F. Haneef, Nikolas J. Podraza, Moses H. W. Chan, V. Gopalan, Karin M. Rabe & Roman Engel-Herbert. Correlated metals as transparent conductors. Nat. Mater. 15 (2016) 204-210.
14. L. Hu, R. Wei, J. Yan, D. Wang, X. Tang, X. Luo, W. Song, J. Dai, X. Zhu, C. Zhang, Y. Sun, $La_{2/3}Sr_{1/3}VO_3$ Thin Films: A New p-Type Transparent Conducting Oxide with Very High Figure of Merit. Adv. Electron. Mater. 4 (2018) 1700476.
15. L. Hu, M.L. Zhao, S. Liang, D.P. Song, R.H. Wei, X.W. Tang, W.H. Song, J.M. Dai, G. He, C.J. Zhang, X.B. Zhu, Y.P. Sun, Exploring High-Performance p-Type Transparent Conducting Oxides Based on Electron Correlation in V_2O_3 Thin Films. Phy. Rev. App. 12 (2019) 044035.
16. Jing Wang, Jingbo Li, and Shu-Shen Li. Native p-type transparent conductive CuI via intrinsic defects. J. Appl. Phys. 110 (2011) 054907.
17. D. Chen, Y. Wang, Z. Lin, J. Huang, X. Chen, D. Pan, F. Huang. Growth strategy and physical properties of the high mobility p-type CuI crystal. Cryst. Growth. Des. 10 (2010) 2057-2060.
18. Y. Li, J. Sun, David J. Singh, Optical and electronic properties of doped p-type CuI: Explanation of transparent conductivity from first principles. Phy. Rev. Mater. 2 (2018) 035003.
19. G. Takenari, T. Tadatoshi, and U. Masayasu, Exciton Luminescence of CuCl, CuBr and CuI Single Crystals. J. Phys. Soc. Jpn. 24 (1968) 314-327.
20. M. Xia, M. Gu, X. Liu, Electrical and luminescence properties of Zn^{2+} doped CuI thin films. J Mater Sci: Mater. Electron. 26 (2015) 2629-2633.
21. C. Yang, D. Souchay, M. Kneiß, M. Bogner, H.M. Wei, M. Lorenz, O. Oeckler, G. Benstetter, Y.Q. Fu, M. Grundmann, Transparent flexible thermoelectric material based on non-toxic earth-abundant p-type copper iodide thin film. Nat. Commun. 8 (2017) 16076.
22. P. Storm, M. S. Bar, G. Benndorf, S. Selle, C. Yang, H. von Wenckstern, M. Grundmann and M. Lorenz, High mobility, highly transparent, smooth, p-type CuI thin films grown by pulsed laser deposition. App. Phy. Lett. Mater. 8 (2020) 091115.
23. Y. Peng, N. Yaacobi-Gross, A. K. Perumal, H. A. Faber, G. Vourlias, P. A. Patsalas, D. D. C. Bradley, Z.He and T. D. Anthopoulos, Efficient organic solar cells using copper(I) iodide (CuI) hole transport layers. App. Phy. Lett. 106 (2015) 243302.
24. M. Kneiß, C. Yang, J. Barzola-Quiquia, G. Benndorf, H. von Wenckstern, P. Esquinazi, M. Lorenz, and M. Grundmann, Suppression of Grain Boundary Scattering in Multifunctional p-Type Transparent γ-CuI Thin Films due to Interface Tunneling Currents. Adv. Mater. Interfaces 5 (2018) 1701411.
25. N. Yamada, R. Ino, and Y. Ninomiya, Truly Transparent p-Type γ-CuI Thin Films with High Hole Mobility. Chem. Mater. 28 (2016) 4971-4981.

26. F. Scheina, H. von Wenckstern, M. Grundmann, Transparent p-CuI/n-ZnO heterojunction diodes. Appl. Phys. Lett. 102 (2013) 092109.
27. J. Chaand, D. Jung. Air-Stable Transparent Silver Iodide–Copper Iodide Heterojunction Diode. ACS Appl. Mater. Interfaces 9 (2017) 43807-43813.
28. M. Cota-Leal, D. Cabrera-German, M. Sotelo-Lerma, M. Martínez-Gil, J. A. García-Valenzuela, Highly-transparent and conductive CuI films obtained by a redirected low-cost and electroless two-step route: Chemical solution deposition of CuS_2 and subsequent iodination. Materials Science in Semiconductor Processing 95 (2019) 59-67.
29. H. Rachel, L. M. Davis, D. Chua, C. M. Chang, and R. G. Gordon, Vapor Deposition of Transparent, p-Type Cuprous Iodide Via a TwoStep Conversion Process. ACS Appl. Energy Mater. 1 (2018) 6953–6963.
30. V. Raj, T. Lu, M. Lockrey, R. Liu, F. Kremer, L. Li, Y. Liu, H. H. Tan, and C. Jagadish, Introduction of TiO_2 in CuI for Its Improved Performance as a p-Type Transparent Conductor. ACS Appl. Mater. Interfaces 11 (2019) 24254-24263.
31. Z. Zheng, A. Liu, S. Wang, B. Huang, K. W. Wong, X. Zhang, S. Hark and W. Lau, Growth of highly oriented (110) γ-CuI film with sharp exciton band. J. Mater. Chem. 18 (2008) 852-854.
32. W. J. Li, E. W. Shi, Growth Habit and Habit Variation of γ-CuI Crystallites under Hydrothermal Conditions. Cryst. Res. Technol. 37 (2002) 1041-1048.
33. K. Watanabe, Kinetics of Solid-State Reaction of BaO_2 and a-Fe_2O_3. J. Am. Ceram. Soc., 81 [3] (1998) 733-37.
34. E. A. Giess, Equations and Tables for Analyzing Solid-state Reaction Kinetics. J. Am. Ceram. Soc. 46 [8] (1963) 374-76.
35. Y. Chang, M. Kneiβa, M. Lorenza, and M. Grundmann, Room-temperature synthesized copper iodide thin film as degenerate p-type transparent conductor with a boosted figure of merit. PNAS. 113 (2016) 12929-12933.
36. C.C. Kim, H.H. Lee, K.H. Oh, J.Y. Sun, Highly stretchable, transparent ionic touch panel, Science 353 (2016) 682–687.
37. G. Chen, L. Bi, Z. Yang, L. Chen, G. Wang, C. Ye, Water-based purification of ultra- thin silver nanowires toward transparent conductive films with a transmittance higher than 99%, ACS Appl. Mater. Interfaces 11 (2019) 22648–22654.
38. F. Cui, Y. Yu, L. Dou, J. Sun, Q. Yang, C Schildknecht, K Schierle-Arndt, P Yang, Synthesis of ultrathin copper nanowires using tris(trimethylsilyl)silane for high performance and low haze transparent conductors, Nano Lett. 15 (2015) 7610–7615.
39. C. Preston, Z. Fang, J. Murray, H. Zhu, J. Dai, J.N. Munday, L. Hu, Silver nanowire transparent conducting paper-based electrode with high optical haze, J. Mater. Chem. C 2 (2014) 1248–1254.
40. K.W. Seo, J. Lee, J. Jo, C. Cho, J.Y. Lee, Highly efficient (>10%) flexible organic solar cells on PEDOT-free and ITO-free transparent electrodes, Adv. Mater. 31 (2019) 1902447–1902452.

41. J. Liao, M. Yang, W. Liu, Y. Zhou, X. Bi, H. Yuan, Green full polymer flexible transparent elextrodes showing versatile switching behaviors based on either counterion transport or nanoarea crystallization, J. Mater. Chem. A 7 (2019) 12825–12832.
42. G. Haacke, New figure of merit for transparent conductors. J. Appl. Phys. 47 (1976) 4086-4089.
43. M. Aksit, S. K. Kolli, I. M. Slauch, R. D. Robinson, Misfit layered $Ca_3Co_4O_9$ as a high figure of merit p-type transparent conducting oxide film through solution processing, Appl. Phys. Lett. 104 (2014) 161901.
44. B. Gunning, J. Lowder, M. Moseley, W. A. Doolittle, Negligible carrier freeze-out facilitated by impurity band conduction in highly p-type GaN, Appl. Phys. Lett. 101 (2012) 082106.
45. E. Fortunato, R. Barros, P. Barquinha, V. Figueiredo, S. K. Park, C. Hwang, R. Martins, Transparent p-type SnO_x thin film transistors produced by reactive rf magnetron sputtering followed by low temperature annealing, Appl. Phys. Lett. 97 (2010) 052105.
46. L. Farrell, K. Fleischer, D. Caffrey, D. Mullarkey, E. Norton, and I. V. Shvets, Conducting mechanism in the epitaxial p-type transparent conducting oxide Cr_2O_3: Mg, Phys. Rev. B 91 (2015) 125202.
47. F.J. Geng, L. Yang, B. Dai, S. Guo, G. Gao, L.G. Xu, J.C. Han, A. Bolshakova, J.Q. Zhu, Simultaneous optimization of transmittance and resistivity for γ-CuI thin films via an iodination method at mild reaction condition, Surface & Coatings Technology 360 (2019) 269-275.
48. M. Wang, H. Wei, Y. Wu, C. Yang, B. Cao, Highly transparent and conductive γ-CuI films grown by simply dipping copper films into iodine solution, Physica B: Condensed Matter 573 (2019) 45-48.
49. D.K. Kaushik, M. Selvaraj, S. Ramu, A. Subrahmanyam, Thermal evaporated copper iodide (CuI) thin films: a note on the disorder evaluated through the temperature dependent electrical properties, Sol. Energy Mater. Sol. Cells 165 (2017) 52-58.
50. C. Yang, M. Kneiß, F.-L. Schein, M. Lorenz, M. Grundmann, Room-temperature Domain-epitaxy of Copper Iodide Thin Films for Transparent CuI/ZnO Heterojunctions with High Rectification Ratios Larger than 109, Scientific Reports 6 (2016) 21937.
51. M.N. Amalina, Y. Azilawati, N.A. Rasheid, M. Rusop, The properties of Copper (I) Iodide (CuI) thin films prepared by Mister Atomizer at different doping concentration, Procedia Eng. 56 (2013) 731-736.

Figures

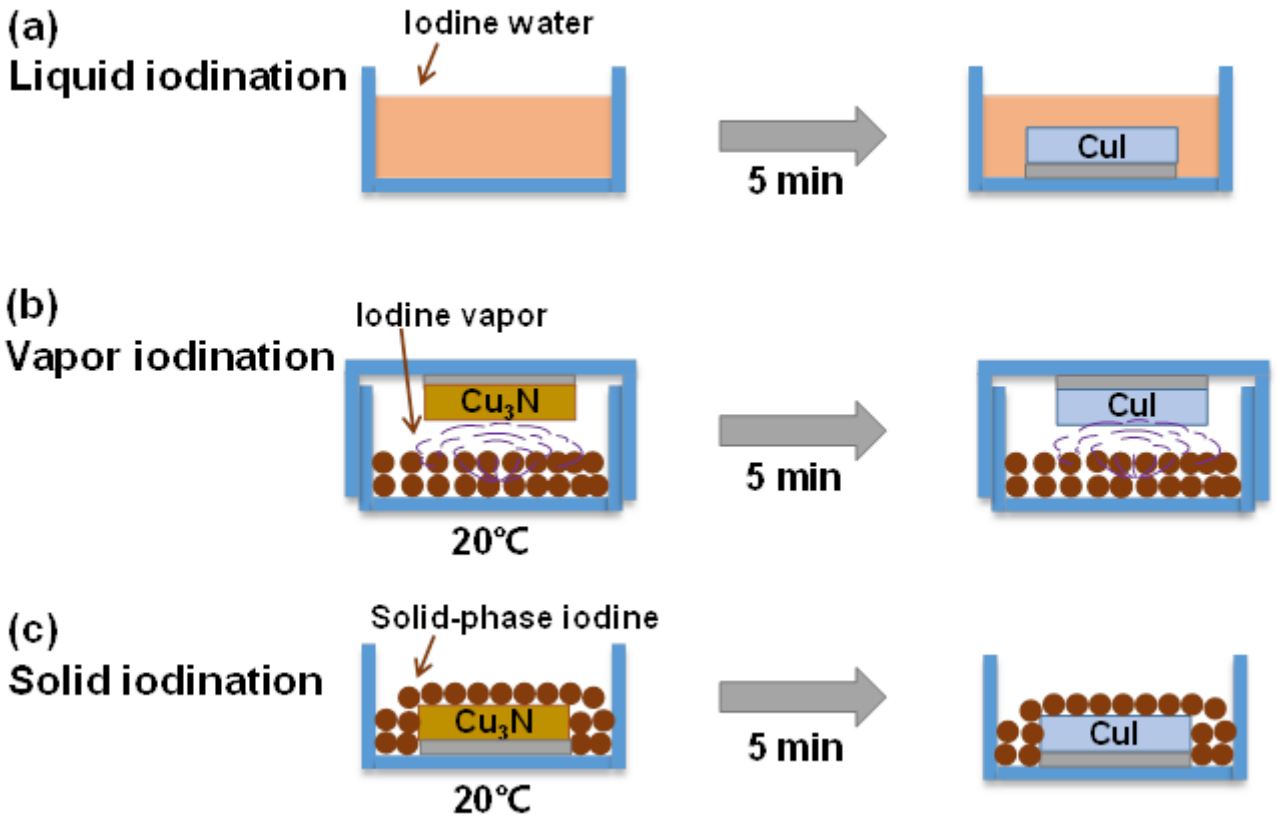

Figure 1

Schematic illustrations of the (a) liquid iodination method (b) vapor iodination method and (c) solid iodination method.

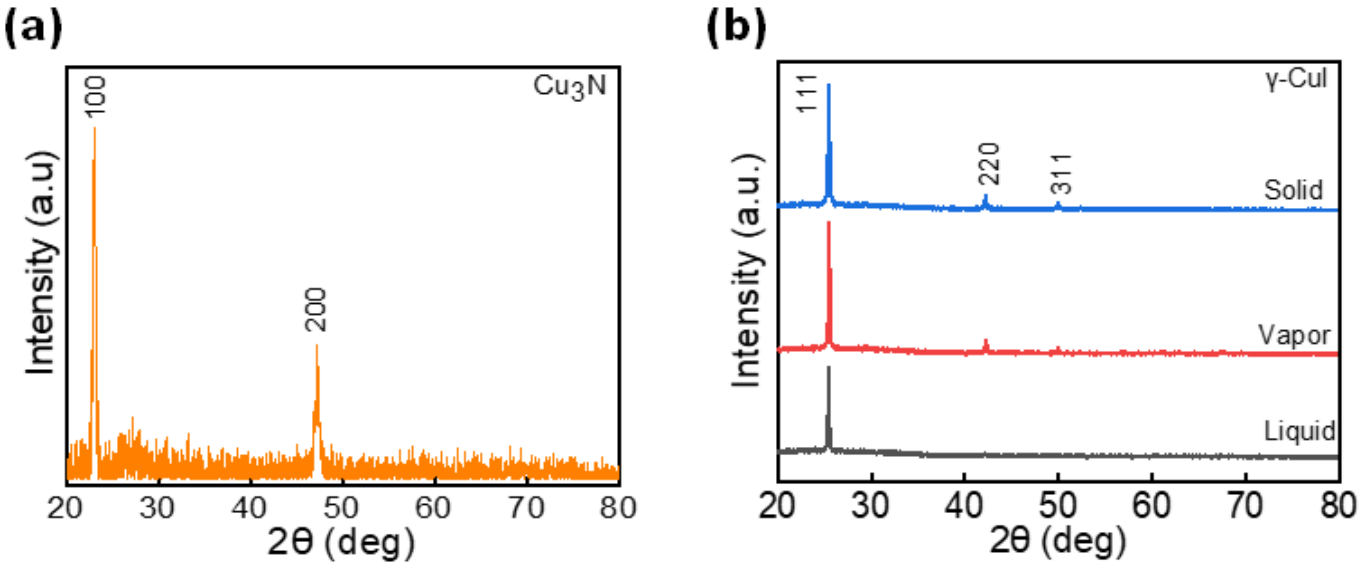

Figure 2

XRD patterns of (a) Cu3N precursor and (b) as-prepared γ-CuI films fabricated via liquid iodination method (grey line) vapor iodination method (red line) and solid iodination method (blue line).

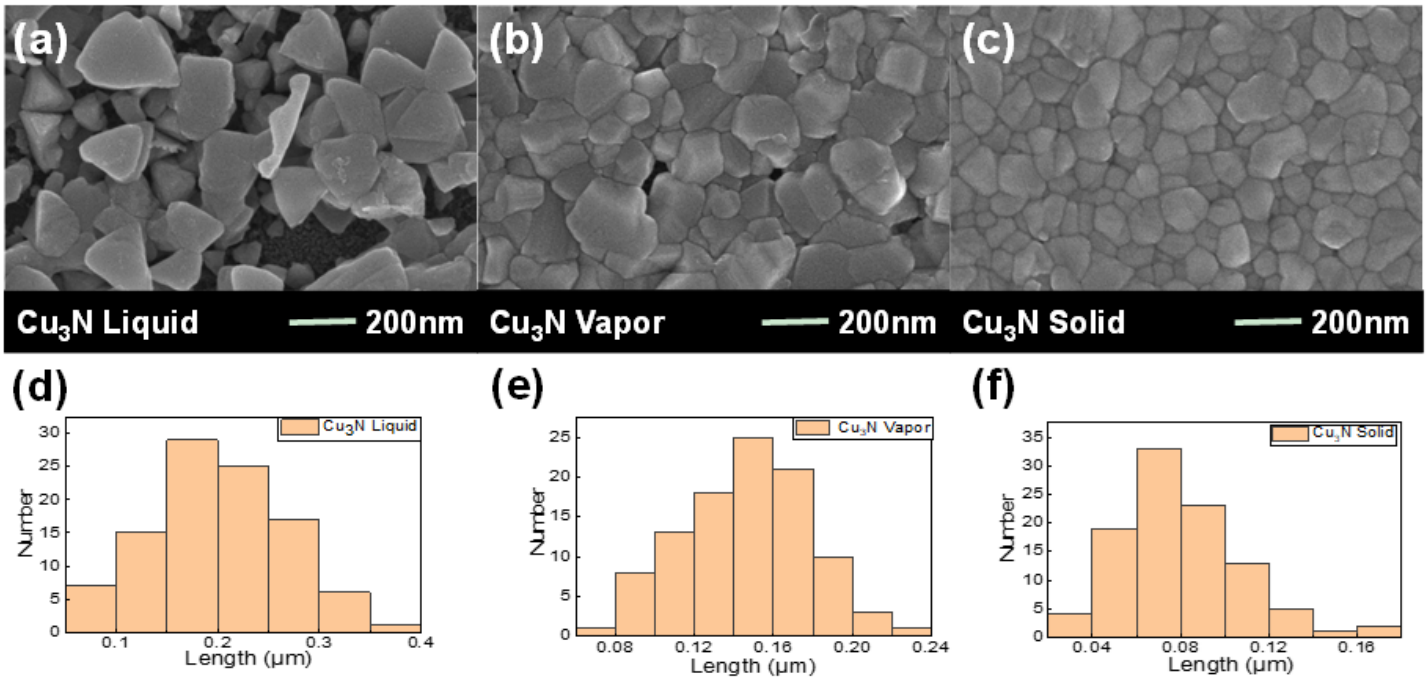

Figure 3

SEM images of γ-CuI films fabricated by (a) liquid method (b) vapor method and (c) solid method. Grain size distribution of γ-CuI films fabricated by (d) liquid method (e) vapor method and (f) solid method.

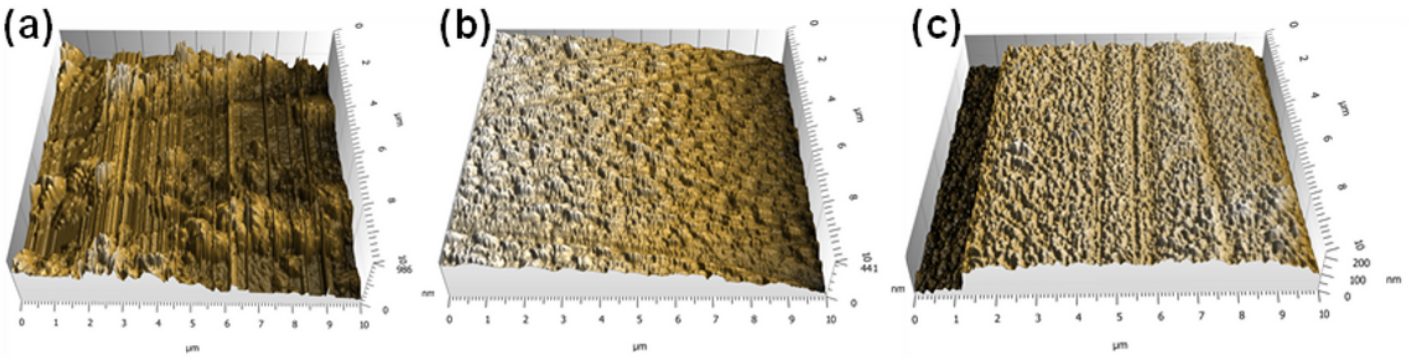

Figure 4

AFM images of γ-CuI films fabricated by (a) liquid method (b) vapor method and (c) solid method.

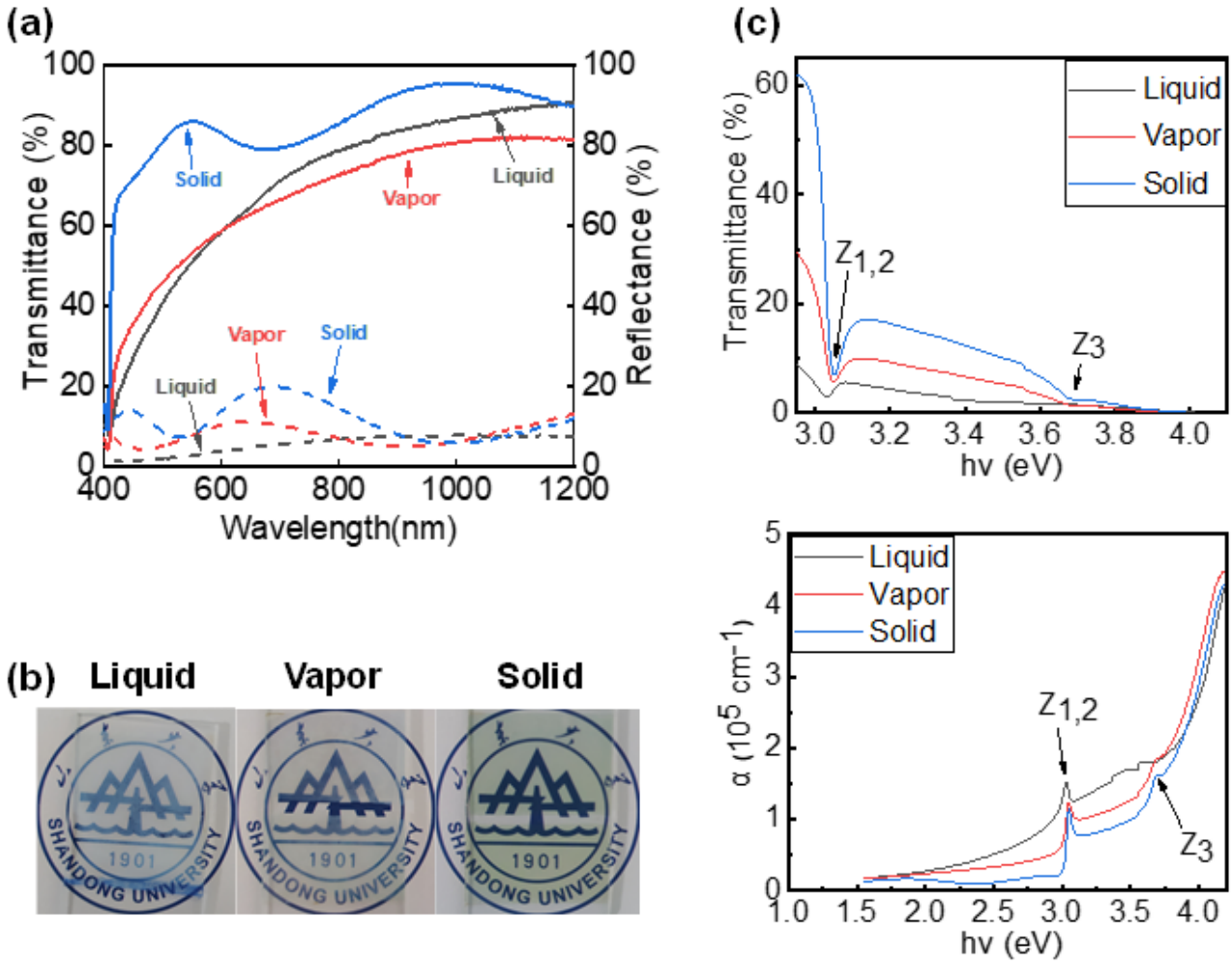

Figure 5

(a) The Vis-IR spectra and (b) the photographs of CuI films fabricated by liquid, vapor, and solid iodination methods, (c) the transmittance and the absorption coefficient as a function of the photon energy of CuI films prepared with different iodination methods. The films fabricated from Cu3N had a thickness of ~220 nm.

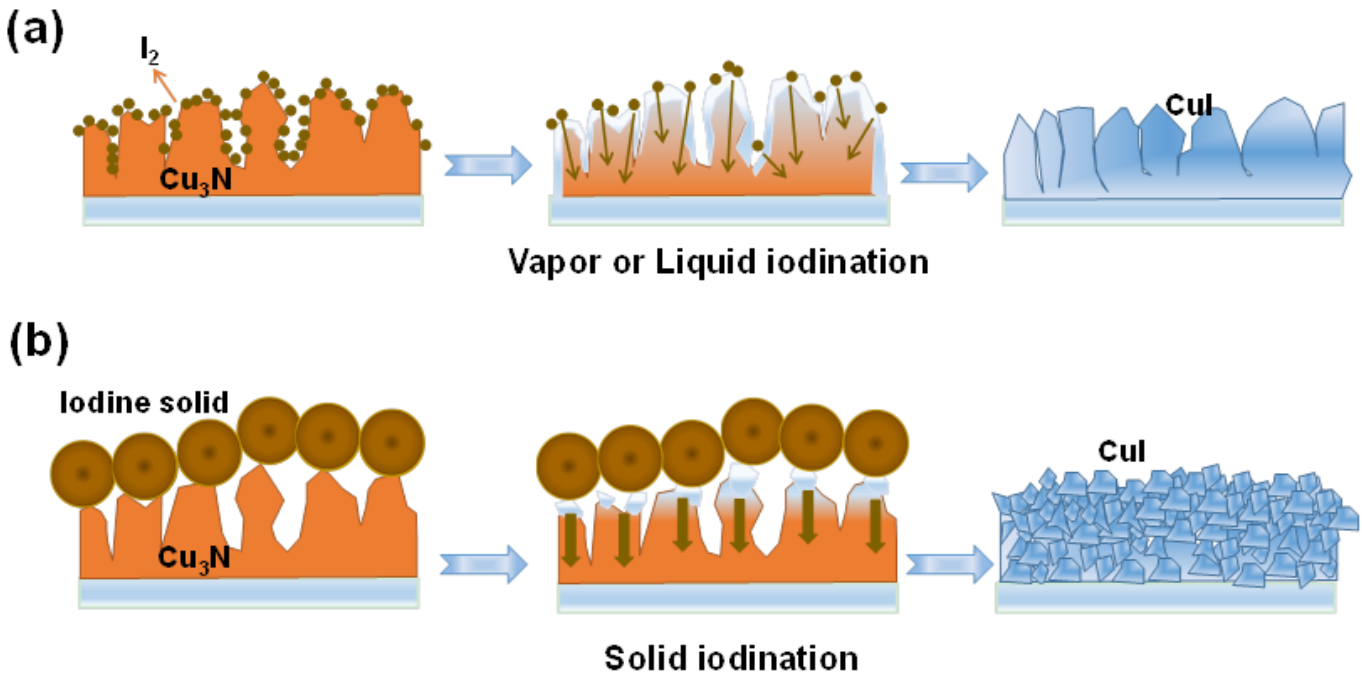

Figure 6

Schematic illustrations of iodination process for (a) vapor, liquid, and (b) solid iodination methods.

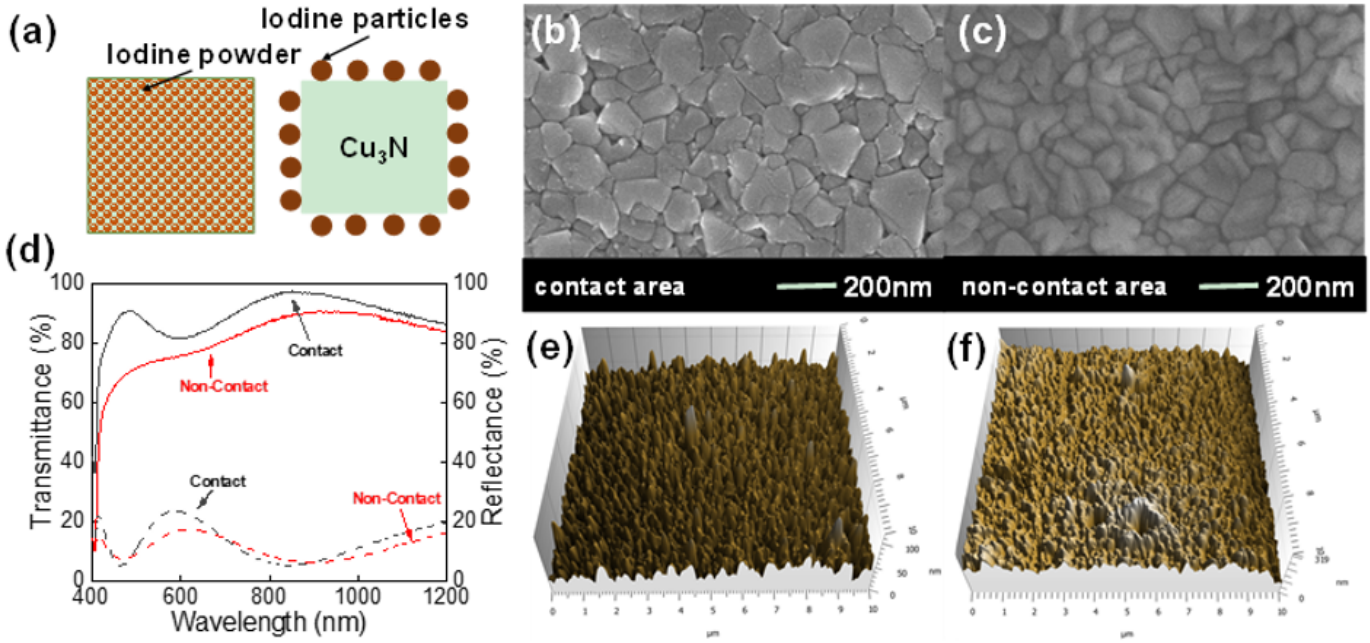

Figure 7

(a) Schematic illustrations of contact iodination process and non-contact process (the right is contact area, the right is the non-contact area) (b)(c) SEM images of solid iodination in the contact area and non-

contact area (d) Comparative UV-vis-IR spectra for two processes and (e)(f) SEM images of solid iodination in the contact area and non-contact area.

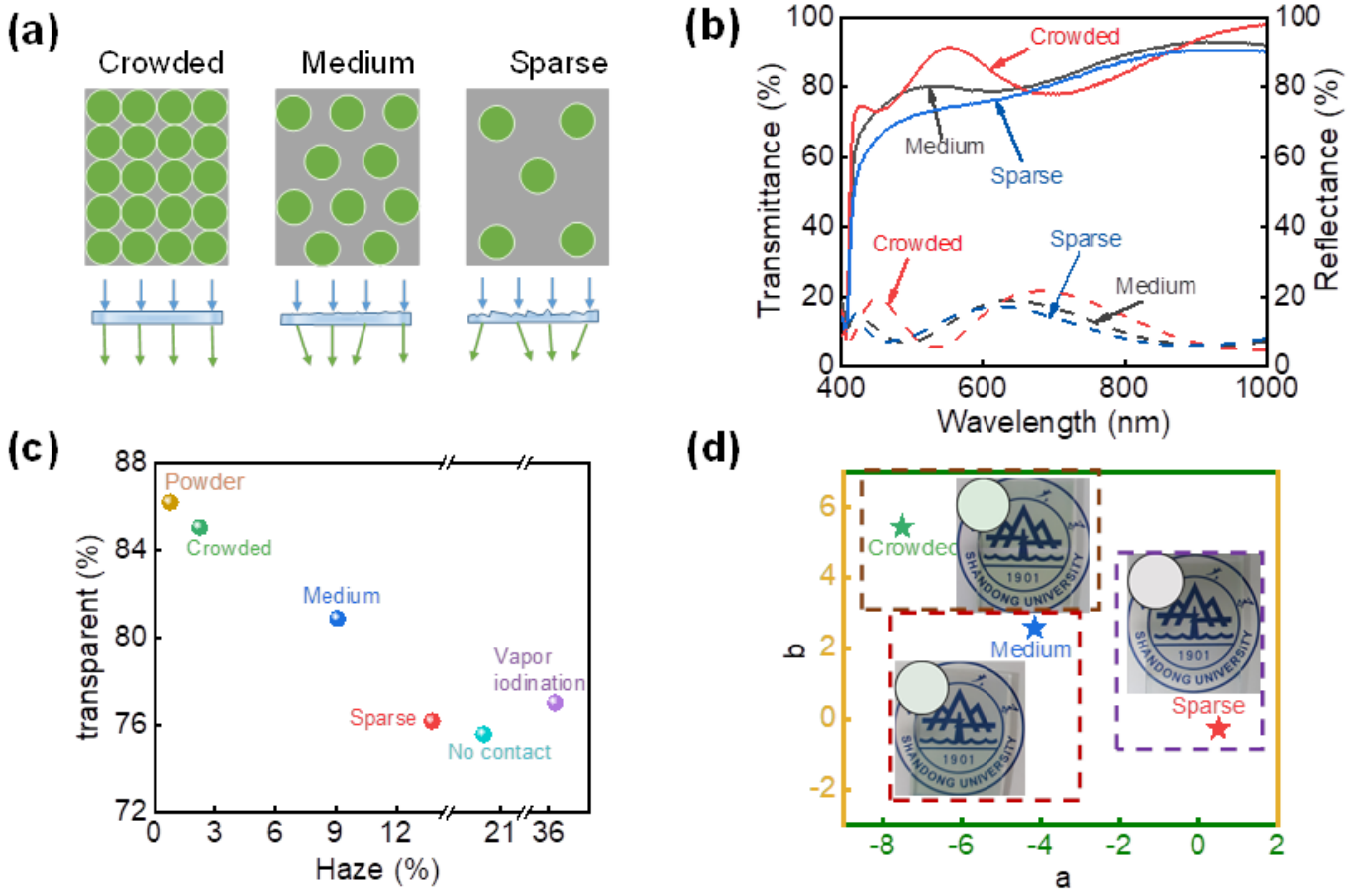

Figure 8

(a) Schematic illustrations of three arrangements and their scattering, the green area represents contact areas, the gray area represents no contact area (b) Comparative UV-vis-IR spectra for three arrangements (c) Comparative visible transparent and haze for three arrangements, contact, no contact, and vapor iodination and (d) Comparative Lab color for three arrangements, the images (inside) are the color corresponding to the LAB color values and photographs. The films have a thickness of ~240 nm.

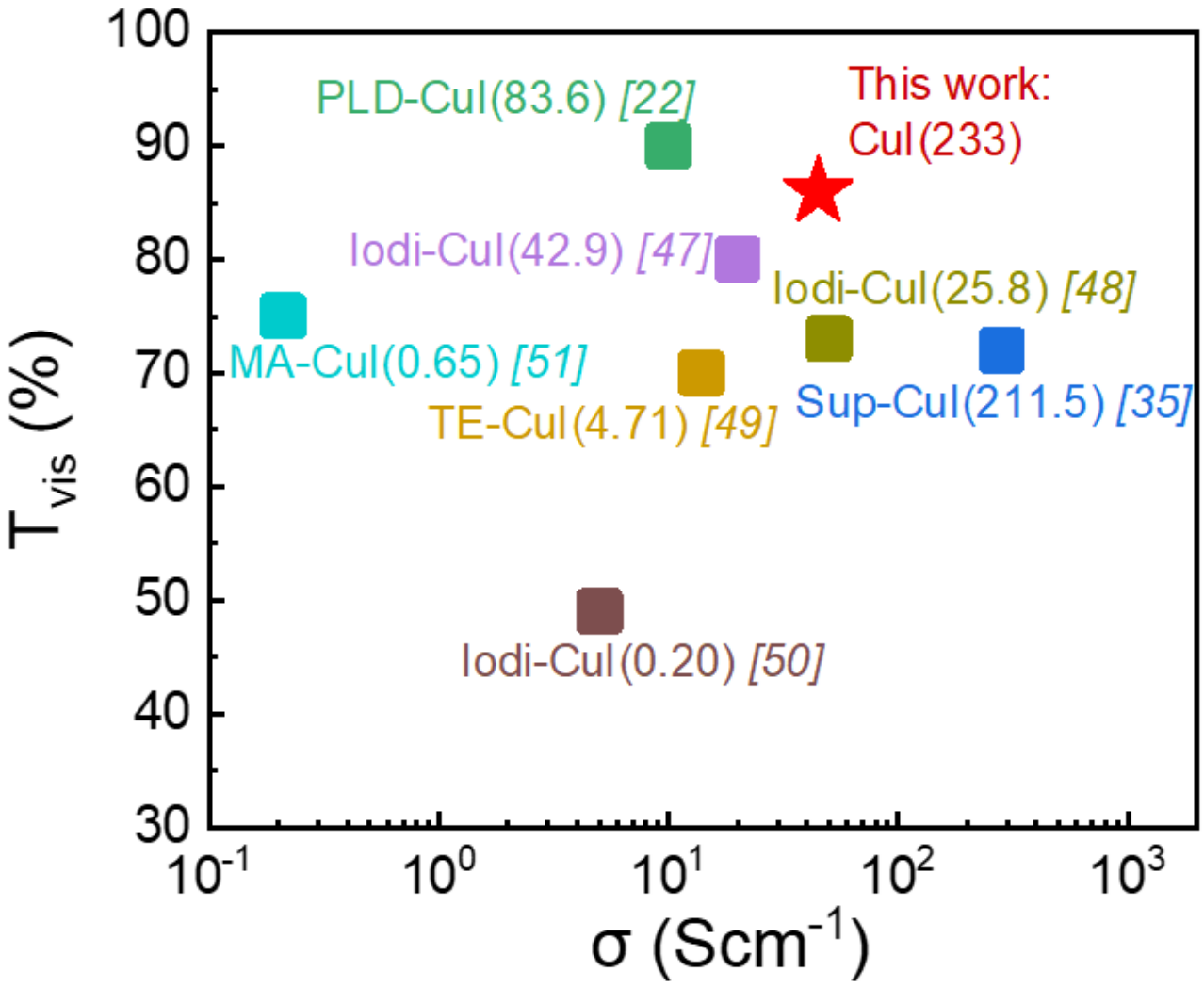

Figure 9

Figures of merit. Graphical representation of electrical resistance, optical transmission, and FOM for as-prepared CuI films (red star) and other CuI films (PLD-CuI: Preparation of CuI films by pulsed laser deposition, Iodi-CuI: Preparation of CuI films by iodination, Sup-CuI: Preparation of CuI films by sputtering, TE-CuI: Preparation of CuI films by thermal evaporation, MA-CuI: Preparation of CuI films by mister atomizer).